JOURNAL OF SOLID STATE CHEMISTRY **141,** 191–198 (1998)
ARTICLE NO. SC987946

Synthesis of Doped and Undoped Nanopowders of Tetragonal Polycrystalline Zirconia (TPZ) by Spray-Pyrolysis

E. Djurado[1] and E. Meunier

Laboratorie d'Electrochimie et de Physico-Chimie des Matériaux et des Interfaces, Institut National Polytechnique de Grenoble (CNRS UMR 5631), associé à l'UJF, B. P. 75, 1130 rue de la Piscine, 38402 St. Martin d'Hères Cedex, France

Received February 13, 1998; in revised form June 24, 1998; accepted July 2, 1998

This work is focused on the synthesis of nanocrystallized tetragonal polycrystalline zirconia (TPZ) powders by the spray-pyrolysis method. A design of experiment (DOE) was used with doped zirconia (2YSZ) to understand the influence of four spray-pyrolysis parameters on the crystallization of TPZ: solution concentration, atomizing frequency, carrier gas flow rate, and furnace temperature. Experimental conditions of the spray pyrolysis method were then selected on the DOE basis, in order to synthetize tetragonal undoped zirconia powders (0YSZ) with well controlled crystallite size. Smallest and largest averaged crystallite sizes of 0YSZ obtained by this method were 6.9 and 13.2 nm, respectively. Their influence on the microstructure of TPZ is characterized by XRD and Raman spectroscopy. Morphology, particle size, and particle size distribution were studied using SEM and granulometry. Nanocrystallization was observed by TEM.

1. INTRODUCTION

Tetragonal zirconia (t-ZrO_2) is stable in the 1170–2370°C temperature range in the ZrO_2 rich region of the ZrO_2–Y_2O_3 phase diagram (1). However, t-ZrO_2 is metastable when it is synthetized at lower temperatures. Up to now, the mechanisms controlling the metastability of the high temperature phases at low temperature remain poorly understood. Garvie and coworkers (2) used surface energy arguments to explain the occurrence of metastable zirconia for nanoparticles smaller than 30 nm. Mitsuhashi *et al.* (3) added strain energy considerations to the surface energy theory and predicted a critical tetragonal crystallite size of 10 nm. This was attributed to the presence of boundary domains between monoclinic and tetragonal zirconia within the polycrystalline particles. These boundaries reduced the driving force for the martensitic trasformation. Osendi (4) and co-workers argued that the presence of anion defects rather than impurities during crystallization was linked to the nucleation of t-ZrO_2. It is found that the addition of MgO, CaO, Y_2O_3, or certain rare-earth oxides to the ZrO_2 matrix stabilizes the tetragonal form. Déchamps *et al.* (5) reported that fine internal porosity in zirconia powders prepared by sol-gel techniques helped stabilize tetragonal zirconia. Another key parameter in the stabilization of the t-ZrO_2 (6) is water vapor which enhances crystallite growth and decreases surface energy.

Tetragonal polycrystalline zirconia (TPZ) can be prepared using various techniques. This work reports the preparation of TPZ at low temperature (~ 600°C) by spray-pyrolysis using an ultrasonic mist generator. The aim of this work is to understand the relationship between the processing parameters, and the crystallite size as well as the dopant contribution to the synthesis of TPZ. A design of experiment (DOE) was used with 2 mol% yttria stabilized zirconia (2YSZ) to understand the influence of four spray-pyrolysis parameters on the crystallization of TPZ. We used the DOE results to predict the minimum crystallite size of 2YSZ obtained by the spray pyrolysis method. The model validity was confirmed with the synthesis of undoped tetragonal zirconia, noted 0YSZ.

2. EXPERIMENTAL SECTION

2.1. Powder Preparation

The 2YSZ and 0YSZ zirconia powders were prepared by the spray-pyrolysis technique using an ultrasonic atomizer. The precursor solutions were prepared from a stoichiometric mixture of zirconyl nitrate hydrate ($ZrO(NO_3)_2$, ALDRICH) and yttrium nitrate ($Y(NO_3)_3$, ALDRICH) in distilled water. A second batch of precursor solution consisted solely of dissolved zirconyl nitrate hydrate. The concentrations investigated were 2.5×10^{-2} and 5×10^{-2} mol.l^{-1}. The solutions were atomized by a high-frequency ultrasonic mist generator. In this study, we used two piezoelectric ceramic transducers for which the frequencies were respectively 850 kHz and 1.7 MHz. The carrier gas ($N_2 + O_2$

[1]Author to whom correspondence should be addressed. E-mail: Elisabeth.Djurado@lepmi.inpg.fr.

0022-4596/98 $25.00

mixture) carried the aerosol through a tubular furnace, 60 mm in diameter and 1090 mm in heated length, with flowrates of 3 l.min^{-1} and 6 l.min^{-1}.

The three-zone pyrolysis furnace (CARBOLITE, TZF 1000°C, Type 7000 W, 30 A, 1 phase) was programmed at 550°C or 750°C, always with a 50°C temperature gradient in the first zone in comparison with the second and the third zones, so as to avoid a too-fast evaporation of the solvent within the droplets. This favors the formation of dense particles. The second and the third zones were heated at the same temperature, at either 600°C or 800°C. The lower temperature limit of 600°C was imposed by the decomposition temperature of the nitrate precursors. One experiment was carried out at 900°C with 0YSZ, the upper temperature limit for the furnace. Table 1 summarizes the experimental conditions.

2.2. Process Optimization

As mentioned earlier, a DOE was used to perform an optimal number of experiments in order to quantify the influence of four processing parameters on TPZ crystallite size. These parameters were: the precursor solution concentration (C, mol.l^{-1}), the atomizing frequency (f, kHz), the carrier gas flowrate (D, l.min^{-1}), and the furnace temperature (T, °C).

Each parameter was tested for an upper and a lower value (Table 1) and a linear model with only first-order interactions between the parameters was postulated for the crystallite size evolution,

$$Y = b0 + \_bi\, Xi + \_bij\, XiXj,$$

where Y is the crystallite size, bn are the model coefficients, and Xm are the parameters.

Sixteen experiments (Table 2) were therefore carried out according to an L_{16} Tagushi table and computer calculations (Echip Software System) assessed the model validity for 2YSZ. This DOE enabled us to tell which parameters are the most influencing of crystalline growth. Table 3 shows the optimal spray-pyrolysis conditions in order to obtain the smallest crystallites.

Finally, we tested the model trends with 0YSZ.

TABLE 2
DOE Parameters and Resulting Crystallite Sizes for 2YSZ Powders

Experiment no.	C (mol.l^{-1})	D (l.min^{-1})	f (kHz)	T (°C)	Crystallite size (nm)
1	5×10^{-2}	6	1.7×10^{3}	800	10.4
2	5×10^{-2}	6	1.7×10^{3}	600	7.5
5	5×10^{-2}	3	1.7×10^{3}	800	10.4
6	5×10^{-2}	3	1.7×10^{3}	600	7.9
9	2.5×10^{-2}	6	1.7×10^{3}	800	9.5
10	2.5×10^{-2}	6	1.7×10^{3}	600	6.2
13	2.5×10^{-2}	3	1.7×10^{3}	800	10.7
14	2.5×10^{-2}	3	1.7×10^{3}	600	7
3	5×10^{-2}	6	850	800	9.4
4	5×10^{-2}	6	850	600	6.5
7	5×10^{-2}	3	850	800	9.2
8	5×10^{-2}	3	850	600	7.4
11	2.5×10^{-2}	6	850	800	10.1
12	2.5×10^{-2}	6	850	600	6.3
15	2.5×10^{-2}	3	850	800	10.6
16	2.5×10^{-2}	3	850	600	7.2

The samples are identified by xYSZ-y in the notation, where x is the mol% of Y_2O_3 and y is the experiment number.

2.3. Powder Characterization

Room temperature Raman spectra were recorded using a DILOR XY multichannel spectrometer provided with a CCD detector. The 514.53 nm (green) excitation line of an argon ion laser was used. All experiments were carried out using a laser power of 20 mW. Positions and full width at half maximum (FWHM) of Raman bands were obtained by deconvolution of Lorentzian-shaped peaks with PeakFit software (v 4.0, Jandel Scientific).

X-ray diffraction patterns were obtained with a Siemens D500 $\theta/2\theta$ diffractometer using the Bragg Brentano geometry (0.03° in 2θ step, 12 s as a counting time) equipped with a rear monochromator (Cu$K\alpha_1$ radiation, $\lambda = 1.5406$ Å). Silicon was used as the internal reference for all scans in

TABLE 1
Spray Pyrolysis Parameters

Solution concentration C (mol.l^{-1})	Atomizing frequency f (kHz)	Carrier gas flow rate D (liter.min^{-1})	Furnace temperature T (°C)
2.5×10^{-2}	850	3	600
5×10^{-2}	1.7×10^{3}	6	800

TABLE 3
Optimal Spray-Pyrolysis Conditions for the Obtention of the Smallest Crystallites

Crystallite size (nm)	Concentration (mol.l^{-1})	Frequency (MHz)	Flow rate (l.min^{-1})	Temperature (°C)
↓	~	↑	↑	↓
6.2	2.5×10^{-2}	1.7	6	600

order to precisely measure the zero shift and the instrumental resolution. Positions and FWHM of XRD peaks were determined by deconvolution of pseudo-Voigt-shaped peaks with ABFit software (ILL, Grenoble, France). TPZ crystallite sizes were calculated using the Debye–Scherrer equation, corrected with silicon for the 111 and 222 peaks of tetragonal zirconia. Phases were identified using DIFFRAC-AT software systems (Socabim, Paris). Cell parameter refinements were performed using the software CELREF (by Laugier and Filhol, ILL, Grenoble, France).

The extent of crystallinity of the powders was determined using a JEOL 300CX transmission electron microscopy.

The particle size distribution was measured with a CILAS 1064 LASER granulometer.

Finally, the particle morphology was determined using scanning electron microscopy (LEO S440). Operating conditions are the following: secondary electron detector, 10 mm working distance, and 20 kV accelerating voltage of the filament.

3. RESULTS AND DISCUSSION

3.1. Influence of Spray-Pyrolysis Parameters on 2YSZ Powders

All 2YSZ powders prepared by spray-pyrolysis crystallize into the tetragonal phase as dense and compositionally homogeneous polycrystalline spheres with 0.2 g/h as average powder yield. Most of XRD profiles display broad peaks among which 200, 202, 131, and 400 are not well resolved. As an example, the XRD pattern of 2YSZ-12 is shown in Fig. 1.

The absence of splitting in two diffraction lines, characteristic of the tetragonal structure, may be attributed either to the small crystallite size or to the deviance from the tetragonality with $c/a \approx 1$. Typically, t′-ZrO_2 is characterized by a c/a ratio >1 and t″-ZrO_2's ≈ 1. Cell parameter refinement leads to $a = 0.5101 \pm 7 \times 10^{-4}$ nm and $c = 0.5184 \pm 7 \times 10^{-4}$ nm ($c/a = 1.016 \pm 0.003$) for 2YSZ-12. The cell volume is equal to 0.1349 nm^3. The tetragonal phase was identified by comparison with ZrO_2 obtained at 1020°C (17-923 JCPDS card, Fig. 1). A 6.3 ± 0.3 nm average crystallite size was calculated with the Debye–Scherrer equation, corrected with silicon by deconvoluting pseudo-Voigt 111 and 222 peaks.

Raman spectroscopy mainly confirms the presence of TPZ and a minority of monoclinic zirconia as shown in Fig. 2; 641, 640, 460, 319, 264, and 148 cm^{-1} Raman frequencies of vibration are respectively associated to Eg, A1g, Eg, B1g, Eg, and B1g symmetry modes of TPZ (7, 8). A small doublet of the monoclinic phase is detectable at 178 and 190 cm^{-1}. An amount of 0.95% monoclinic phase was calculated according to a quantitative phase analysis carried out from the intensity ratios by Kim *et al.* (9) using Raman spectroscopy.

A DOE was used for the process optimization to obtain the smallest 2YSZ crystallite sizes. The four processing parameters (solution concentration, atomizing frequency, carrier gas flow rate, and furnace temperature) proved to have quite specific contributions to the final particle micro strucure and morphology.

Spherical particles contain fine crystallites ranging from 6.2 to 10.7 nm in length in the 600°C to 800°C temperature range (16 experiments, Table 2). TEM diffraction diagrams show rings with many small spots characteristic of good

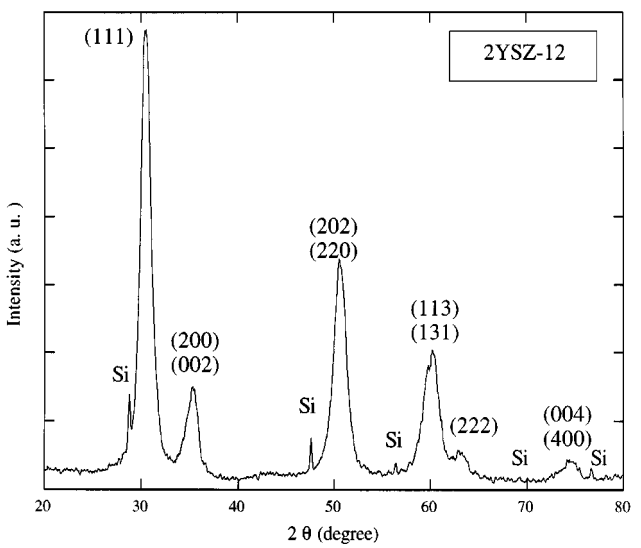

FIG. 1. X-ray diffractogram of 2YSZ-12 powder.

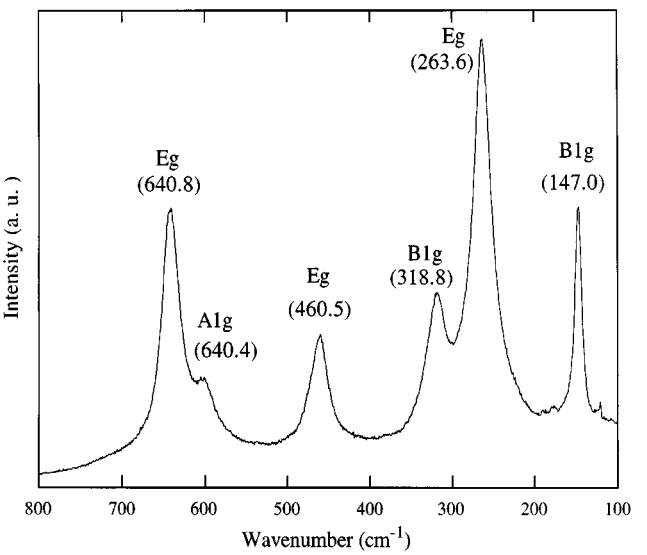

FIG. 2. Raman spectrum of 2YSZ-12 tetragonal zirconia, fired at 800°C for 2h.

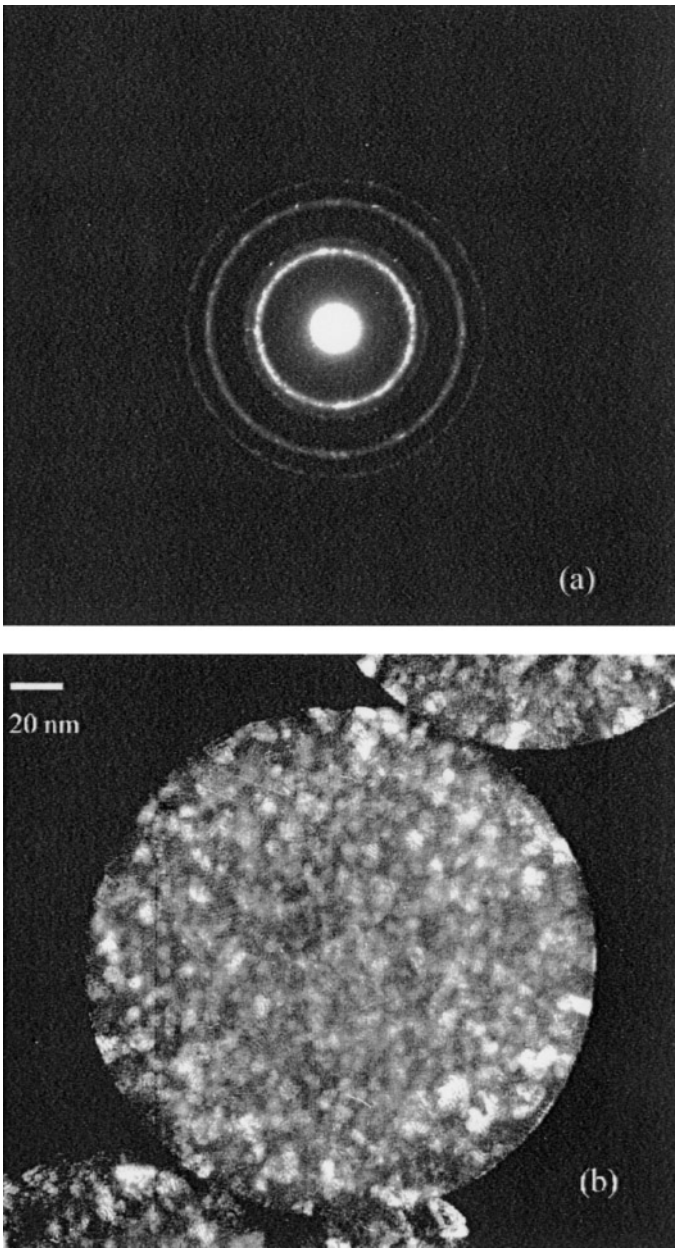

FIG. 3. TEM observations of 2YSZ-12 powder: (a) electron diffraction diagram ($L = 100$ cm); (b) dark field image. Bar indicates 20 nm.

microcrystallization of the powders (Fig. 3a). The diffraction spots were indexed in the tetragonal system. The first intense ring could be indexed as (111) reticular plane, the second weak ring as (200), the third ring with notable intensity as (202), and the weak last one as (131). Dark field imaging (Fig. 3b) confirmed the nano crystallite sizes. Averaged crystallite size measured by TEM (Fig. 3b) and by XRD (Debye–Scherrer equation) are of the same order of magnitude. The majority of particles is dense according to dark field TEM micrographs where crystallites can only be seen on the edges of the particles, the center being opaque to electrons.

Optimal spray-pyrolysis conditions for the smallest 2YSZ crystallites are given in Table 3.

The furnace temperature is the most influential parameter on crystallite growth. This can be attributed to thermally activated diffusion phenomena directly linked to crystal growth. The carrier gas flow rate coupled with the atomizing frequency also influences crystal growth. The atomizing frequency of the ultrasonic atomizer is directly related to the aerosol droplet size (10) according to Eq. [1],

$$d_{\text{th}} = [(\pi.\sigma)/(4\rho\,.f^2)]^{1/3}, \qquad [1]$$

where d_{th} is the theoretical droplet diameter, σ is the surface tension of the liquid, ρ is the solution density, and f is the ultrasonic frequency. This equation shows that low frequencies generate large droplets. Typically, droplet size ranges from 4.3 μm for 850 kHz to 2.7 μm for 1.7 MHz.

Furthermore, we estimated a 17 s residence time of the droplets inside the pyrolysis furnace for a $3\,l.min^{-1}$ flow rate (half as much for $6\,l.min^{-1}$). Thus, slow flowrates increase the residence time for each system within the furnace enhancing diffusion phenomena.

Particle size (polycrystalline spheres) and size distribution were studied by granulometry; d_{10} (diameter of particles at 10 wt% concentration) is 0.3 μm and 0.4 μm, d_{90} is 1.5 μm and 2.3 μm, and d_{50} is 0.8 μm and 0.9 μm, respectively for 2YSZ-3 prepared with a 850 kHz atomizing frequency (Fig. 4, curve a) and for 2YSZ-1 prepared with a 1.7 MHz atomizing frequency (Fig. 4, curve b). Consequently, we suggest that the lower the atomizing frequency, the smaller the size of

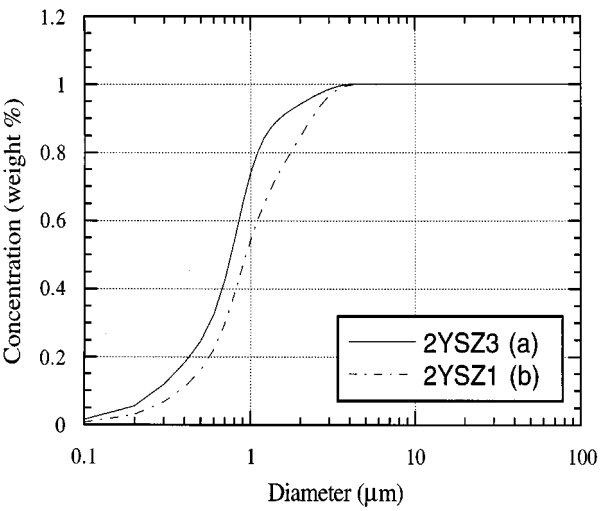

FIG. 4. Added up concentrations of particles versus their diameter in: (a) 2YSZ-3 powder prepared at 850 kHz; (b) 2YSZ-1 powder prepared at 1.7 MHz.

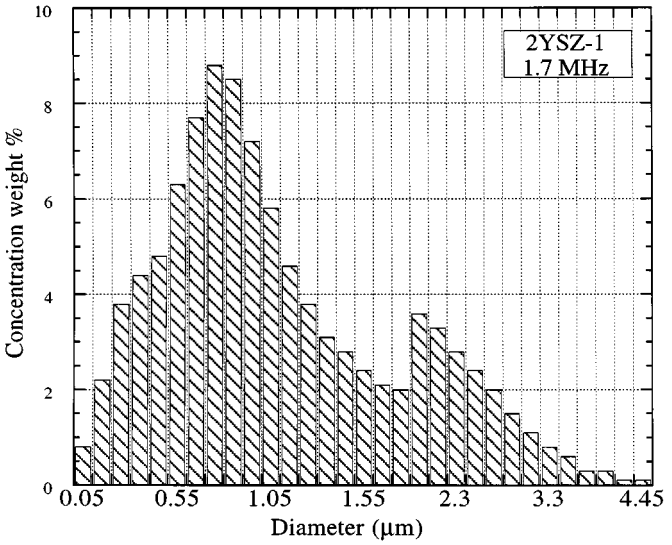

FIG. 5. Histogram showing the size distribution of 2YSZ-1 particles.

nanocrystallized particles. We note a lower dispersion for 2YSZ-3 ($d_{90} - d_{10} = 1.2\ \mu m$) than for 2YSZ-1 ($d_{90} - d_{10} = 2\ \mu m$). As an example, the particle size distribution of sample 2YSZ-1 is shown in Fig. 5. The profile is mainly monodispersed. A smaller secondary peak in the histogram (Fig. 5), around 2.3 μm, is attributed to a small amount of larger particle diameters $> d_{90}$. The SEM micrograph (Fig. 6c) is in good agreement with the particle sizes and size distributions.

Qualitative results were obtained on the particle surface morphology. Four morphologies were observed by SEM (Fig. 6). The main features of these morphologies and their respective experimental conditions are summarized in Table 4. For the three following experiments (Nos. 9, 11, 3; Table 4), the flowrate (D) and the furnace temperature (T) are kept constant at $6\,l.min^{-1}$ and 800°C, respectively.

One morphology consists of smooth and perfectly spherical particles (Fig. 6a) that are obtained using low solution concentration ($2.5 \times 10^{-2}\ mol.l^{-1}$) and high atomizing frequency (1.7 MHz) (experiment 9, Table 4).

Rougher spherical particles (Fig. 6b) result when the frequency parameter is decreased from 1.7 MHz (2.7 μm droplets) to 850 kHz (4.3 μm droplets) (experiment 11, Table 4). The solvent evaporation rate is believed to be responsible for this change. Messing (11) and co-workers described the evaporation stage of the process as a series of physical phenomena occurring simultaneously. They built a model incorporating both solute diffusion and the droplet shrinkage rate (related to the evaporation rate).

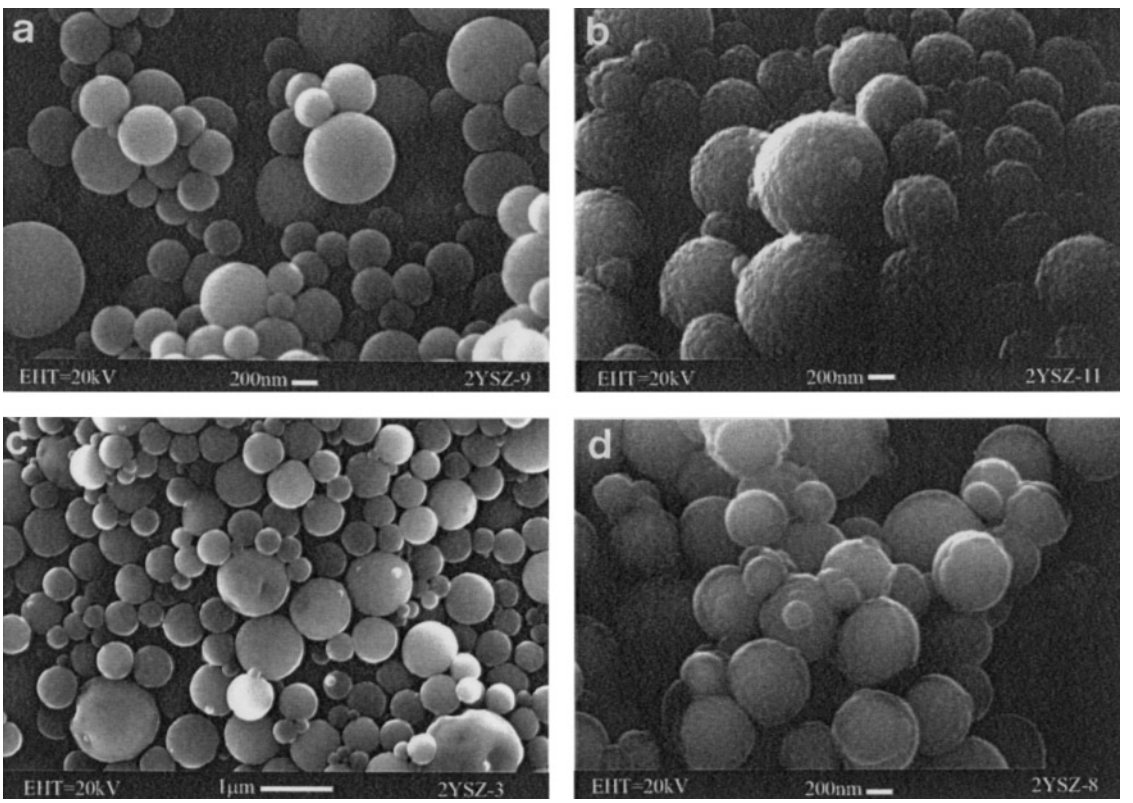

FIG. 6. Four types of morphology observed by SEM: (a) 2YSZ-9; (b) 2YSZ-11; (c) 2YSZ-3; (d) 2YSZ-8.

TABLE 4
Four Types of Morphology as Observed by SEM

Experiment no.	$P_1 : C$ (mol.l^{-1})	$P_2 : D$ (l.min^{-1})	$P_3 : f$ (kHz)	$P_4 : T$ (°C)	Crystallite size (nm)	Morphology SEM
9	2.5×10^{-2}	6	1.7×10^3	800	9.5	Smooth spheres
11	2.5×10^{-2}	6	850	800	10.1	Grain spheres
3	5×10^{-2}	6	850	800	9.4	Smooth spheres Distorted big ones
8	5×10^{-2}	3	850	600	7.4	Multilayered spheres

A third type of morphology appears when solution concentration is raised to 5×10^{-2} mol.l^{-1} (experiment 3, Table 4), wherein smooth but distorted particles (Fig. 6c) result. Indeed, high concentration of the initial solution increases the droplet density which is thereby submitted to high internal stress during particle formation. It is due to rapid evaporation of the solvent from the droplet surface leading to the formation of a salt crust around the particles (12).

Finally, a fourth morphology, wherein agglomerated particles are produced (Fig. 6d), is achieved using a slow flow-rate ($D = 3$ l.mn^{-1}) and a low temperature ($T = 600$°C) while C and f are now constant parameters in relationship with experiment 3 (experiment 8, Table 4).

The main feature of all zirconia particles produced by spray-pyrolysis is that they are dense spheres, contrary to literature reports of hollow spherical shell fragments (12, 13).

However, the link between crystallite growth and particle morphology has to be clarified in the future.

3.2. Undoped TPZ Nanopowders

The optimal experimental conditions obtained from the results of the DOE for 2YSZ were tested on 0YSZ samples prepared by the spray-pyrolysis technique. Fine and very comparable crystallite sizes were achieved for both 2YSZ and 0YSZ powders, respectively, 6.3 ± 0.3 nm and 6.9 ± 0.2 nm (Table 5).

The opposite conditions of the spray-pyrolysis synthesis were then set in order to yield larger crystallites within the 900°C temperature limit of the device. The obtention of 13.2 ± 0.8 nm crystallites was successful. The DOE results were thereby confirmed for undoped zirconia powders since crystallite growth did occur with the temperature increase.

Undoped zirconia crystallizes in tetragonal form, compared to zirconia obtained at 1020°C (No. 17–923 JCPDS card) with averaged crystallite sizes ranging from 6.9 to 13.2 nm (Fig. 7, respectively curve a and curve b). Cell parameter refinement leads to $a = 0.5092 \pm 9 \times 10^{-4}$ nm and $c = 0.5165 \pm 8 \times 10^{-4}$ nm ($c/a = 1.014$) for 0YSZ (6.9 nm) and to $a = 0.50842 \pm 5 \times 10^{-5}$ nm and $c = 0.51859 \pm 5 \times 10^{-5}$ nm ($c/a = 1.020$) for 0YSZ (13.2 nm), compared to $a = 0.512$ nm and $c = 0.525$ nm for ZrO_2 given by No. 17–923 JCPDS card. The unit cell volume is respectively equal to 0.13390 nm^3 for 0YSZ (6.9 nm) and to 0.13405 nm^3 for 0YSZ (13.2 nm). However, the measured variations for 0YSZ (13.2 nm) are not significant since they are of the same order of magnitude as the internal silicon reference. In other words, in this case, the cell variations cannot be precisely measured because they are limited by the instrumental resolution. This is not the case for the two other samples which contain smaller crystallites. For example, the measured cell parameter variations for undoped zirconia (6.9 nm) are 25 times larger than the instrumental resolution. The splitting of the TPZ diffraction lines could only be observed for large crystallite sizes (Fig. 7, curve b). Simultaneously, a low additional *112* peak at $2\theta = 43.3 \pm 0.7°$, characteristic of tetragonal phase, is clearly present. The results of peak deconvolution show that all FWHM of 0YSZ (13.2 nm) are around two times smaller than 0YSZ (6.9 nm).

Raman spectra confirmed the tetragonal 0YSZ phase (Fig. 8, curves a and b). Simultaneous main shifts of two Eg

TABLE 5
DOE Testing Experiments

Composition	Concentration (mol.l^{-1})	Frequency (kHz)	Flow rate (l.min^{-1})	Temperature (°C)	Crystallite size (nm)
2YSZ	2.5×10^{-2}	1.7×10^3	6	600	6.3
0YSZ	2.5×10^{-2}	1.7×10^3	6	600	6.9
0YSZ	2.5×10^{-2}	850	3	900	13.2

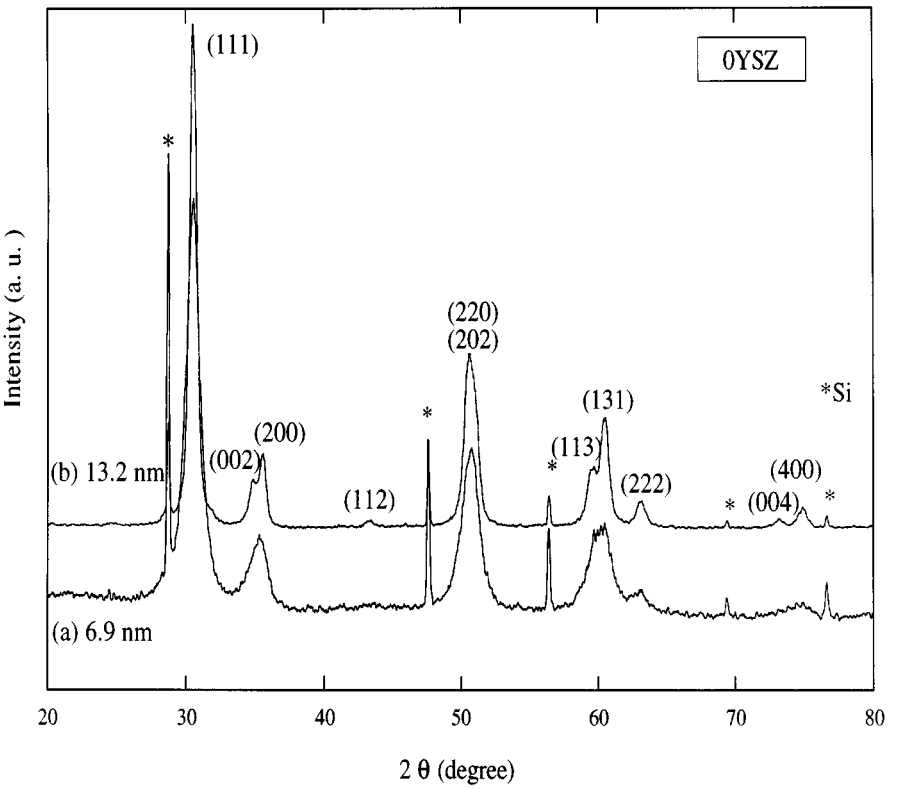

FIG. 7. XRD profiles of two 0YSZ prepared by spray-pyrolysis characterized by (a) 6.9 nm; (b) 13.2 nm, as averaged crystallite sizes.

bands in the opposite direction were observed when the crystallite size of 0YSZ increased from 6.9 nm to 13.2 nm (Table 6). A 4.2 cm^{-1} shift of the Eg frequency position at $\approx 270\ cm^{-1}$ was measured towards lower frequencies while an increase of 2.5 cm^{-1} frequency position of the Eg mode located at around 640 cm^{-1} was detected. These Raman shifts were measured as a function of the applied stress by Anastassakis *et al.* on stabilized tetragonal zirconia (5.3 wt%) (8). These shifts could be attributed to stresses present in the nanocrystallites. Actually, frequency evolution was also detected in nanocrystalline SnO_2 and was interpreted in terms of tensile surface stresses (14). A recent Raman study of nanocrystalline zirconia from Cezus Chimie was carried out using mechanical uni-axial pressure and showed a clear destabilization of TPZ towards the monoclinic phase (15). The sample which contains the largest crystallites exhibits the narrowest Raman lines (Table 6). Further work on the Raman study and X-ray diffraction

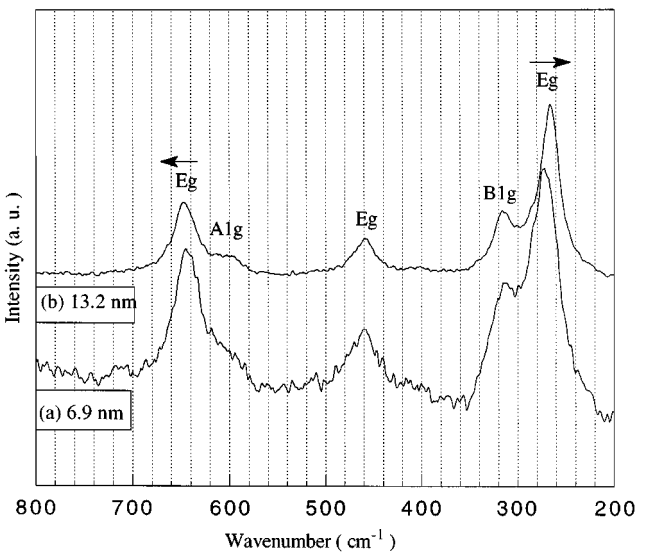

FIG. 8. Raman spectra of 0YSZ prepared by spray-pyrolysis characterized by (a) 6.9 nm; (b) 13.2 nm, as averaged crystallite sizes.

TABLE 6
Positions and Widths of Two Raman Eg Bands versus Crystallite Sizes

Crystallite size (nm)	Center (cm^{-1})	FWHM (cm^{-1})
6.9	270.1	16.8
13.2	265.9	11.1
6.9	643.8	17.1
13.2	646.3	15.3

analysis of structural transition of tetragonal zirconia towards monoclinic phase versus the crystallite size effect will be presented in a forthcoming paper (16).

All our results suggest that the dopant does not play a primary role in the synthesis of TPZ powders at low temperature produced by spray-pyrolysis. Instead, the phase stability is due to the small crystallite sizes achieved by the elaboration process. We believe that the spray-pyrolysis technique is responsible for producing small TPZ crystallites which are stable at room temperature due to surface energy contributions. In his work, Garvie (2) already suggested that surface energy could become predominant in the stabilization of TPZ when pure zirconia crystallites are less than 30 nm in diameter.

4. CONCLUSION

The spray-pyrolysis method mainly provided submicron spherical particles containing nanocrystallites with homogeneity in chemical composition. 2YSZ tetragonal monodispersed powders containing 6.2 to 10.7 nm crystallites were successfully synthetized by this method. A c/a ratio equal to 1.016 ± 0.003 was determined by cell parameter refinement. The crystallite size and particle morphology were controlled using a DOE. Among the spray-pyrolysis parameters, solution concentration has an influence on particle morphology. The carrier gas flow rate affects crystallite growth when it is coupled with the atomizing frequency. The atomizing frequency itself plays a key role on particle size and particle size distribution, but also affects particle morphology. Temperature is, however, the main factor for crystallite growth due to diffusion phenomena. The DOE was successfully applied to undoped zirconia (0YSZ). Small crystallite sizes ranging from 6.3 to 13.2 nm were obtained and the t″-ZrO_2 phase ($c/a \approx 1$) was stabilized as proved by X-ray and Raman measurements.

Results of this study provide further insight into the nature of metastable zirconia.

ACKNOWLEDGMENTS

The authors thank P. Ozil for his help in DOE calculations, N. Rosman for his technical assistance for Raman measurements, and L. Abello, G. Lucazeau, and P. Bouvier for Raman discussions.

REFERENCES

1. H. J. Scott, *J. Mater. Sci.* **10,** 1527 (1975).
2. R. C. Garvie, *J. Phys. Chem.* **69,** 1238 (1965).
3. T. Mitsuhashi, M. Ichihara, and U. Tatsuke, *J. Am. Ceram. Soc.* **57,** 97 (1974).
4. M. I. Osendi, J. S. Moya, C. J. Serna, and J. Soria, *J. Am. Ceram. Soc.* **68,** 135 (1985).
5. M. Déchamps, B. Djuricic, and S. Pickering, *J. Am. Ceram. Soc.* **78,** 2873 (1995).
6. Y. Murase and E. Kato, *J. Am. Ceram. Soc.* **66,** 196 (1982).
7. A. Feinberg and C. H. Perry, *J. Phys. Chem. Solids* **42,** 513 (1981).
8. J. Cai, Y. S. Raptis, and E. Anastassakis, *Appl. Phys. Lett.* **62,** 2781 (1993).
9. B-K. Kim, J-W. Hahn, and K. R. Han, *J. Mater. Sci. Lett.* **16,** 669 (1997).
10. B. Dubois, D. Ruffier, and P. Odier, *J. Am. Ceram. Soc.* **72,** 713 (1989).
11. G. L. Messing, S-C. Zhang, and G. V. Jayanthi, *J. Am. Ceram. Soc.* **76,** 2707 (1993).
12. H. Ishizawa, O. Sakurai, N. Mizutani, and M. Kato, *Am. Ceram. Soc. Bull.* **65,** 1399 (1986).
13. S-C. Zhang, G. L. Messing, and M. Borden, *J. Am. Ceram. Soc.* **73,** 61 (1990).
14. L. Abello, B. Bochu, A. Gaskov, S. Koudryavtseva, G. Lucazeau, and M. Roumyantseva, *J. Solid State Chem.* **135,** 78 (1998).
15. P. Bouvier, D. E. A. Sciences et génie des matériaux, Institut National Polytechnique de Grenoble, 1996.
16. E. Djurado, P. Bouvier, and G. Lucazeau, *J. Solid State Chem.*, in press.